JOURNAL OF CATALYSIS 64, 241–250 (1980)

Pentane Isomerization Kinetics over Nickel-Loaded Y-type Zeolite

P. L. LAW[1] AND C. N. KENNEY

Department of Chemical Engineering, University of Cambridge, Pembroke Street, Cambridge, England

Received November 16, 1977; revised November 26, 1979

The activity of a nickel-loaded Y-type zeolite for the isomerization of *n*-pentane under industrial hydroisomerization conditions was examined. Introduction of the metal by ion exchange and reduction leads to a catalyst with acidic and hydrogenation–dehydrogenation functions. Increasing the nickel loading led to a more than linear increase in the activity and this was seen as being principally due to the accompanying intrazeolitic protons. The rate of isomerization was independent of total pressure, and rate data were obtained at 295, 308, and 319°C. A two-parameter rate equation describing adsorption of the *n*-olefin intermediate onto the intrazeolitic acid sites was found to be adequate in accounting for the rate data. Cracking patterns indicated that formation of light hydrocarbons was by hydrogenolysis over nickel. After reduction the metal component was found to have migrated to the surface of the zeolite crystals and was in a form comprising 25% diffracting nickel crystallites. Selective chemisorption suggested the remaining nickel was finely dispersed, much of it showing monolayer character.

INTRODUCTION

Zeolites containing small quantities of noble metal are now in commercial use as hydroisomerization catalysts (*1*).

There is evidence that reforming isomerizations of *n*-paraffins over the more conventional alumina-based catalysts proceeds via a three-stage sequence involving both noble metal and acidic alumina sites (*2–7*). In this sequence the *n*-paraffin is first converted to the *n*-olefin over the noble metal, after which it isomerizes to the i-olefin over the acidic alumina. A subsequent hydrogenation on the metal produces the i-paraffin.

This work is concerned with the preparation and characterization of a Y-type zeolite containing nickel. The kinetics of the isomerization of *n*-pentane over the catalyst under industrial hydroisomerization conditions are evaluated and the associated cracking patterns observed.

NOMENCLATURE

I	Intensity of diffracted line
W	Weight fraction
R	Observed rate of isomerization (g mole/hr g)
$\hat{R}$	Predicted rate of isomerization (g mole/hr g)
$P_{1,2,3}$	Partial pressure of *n*-pentane, i-pentane, hydrogen (psig)
K_d	Equilibrium constant for *n*-pentane dehydrogenation to *n*-pentene
K_1	Equilibrium constant for isomerization of *n*-pentene
K_h	Equilibrium constant for hydrogenation of i-pentene
$K_{5,6,7}$	Equilibrium constants for substeps within the *n*-pentene isomerization sequence
K	Equilibrium constant for the overall isomerization of *n*-pentane
k	Forward reaction rate constant for a particular substep
X	Concentration of active acid sites (moles/g)
$k_{a,i,d}$	Reaction rate constants for substeps within the *n*-pentene isomerization sequence ($=kX$)
b	Constant in linearized rate equation (g hr/g mole)
ρ	Density (g/cm^3)
μ	Mass absorption coefficient (cm^2/g)

[1] Present address: ICI Agricultural Division, Billingham, Cleveland, England.

0021-9517/80/080241-10$02.00/0

METHODS

Catalyst Preparation and Characterization

All catalysts were prepared by ion exchanging quantities of Linde SK-40, a sodium Y-type zeolite, in aqueous nickel nitrate solution. The cation exchange capacity was calculated to be 3.10×10^{-3} g ions of sodium per g of zeolite, and it was found that a maximum of 66% of the sodium ions were replaceable by nickel ions. The exchanged zeolites were activated by reduction in pure hydrogen at elevated temperature. Nickel dispersion was estimated by selective absorption of CO according to the method of Brooks and Christopher (*8*). Catalyst samples were reduced for 16 hr at 500°C, cooled at 25°C, and equilibrated with carbon monoxide at 300–400 Torr in a conventional BET apparatus. Desorption isotherms were followed down to <100 Torr. Cu$K\alpha$ radiation was employed for the X-ray diffraction.

Catalyst Activity

Reactant conversions were obtained using a tubular flow reactor composed of nonickel steel, designed to operate at temperatures and pressures of up to 500°C and 3.5×10^6 N m^{-2}. The catalyst was situated in a basket at the center of the tube, and a wad of inert glass wool was used to suspend it in its original powder form. Catalyst reductions were carried out *in situ*, and all reaction rates were calculated from differential conversions of 2–8%. External heat and mass transfer resistances were calculated to be negligible for all runs. Rate data could be obtained using three-component mixtures of *n*-pentane, i-pentane, and hydrogen of any desired composition. This was made possible by using a vaporizer containing a mixture of isomers through which hydrogen was bubbled. In order to avoid excessive catalyst deactivation, a high hydrogen/pentanes molar ratio was always maintained when measuring rates. Reactants and products were analyzed with a gas chromatograph equipped with a flame ionization detector and a 7.3-m column containing squalane on diatomite. The peaks were integrated automatically.

RESULTS

Physical Characterization of the Catalyst

XRD powder traces showed that the zeolite matrix remained highly crystalline after reduction. However, a strong diffraction line corresponding to the $d = 2.03$ Å spacing of crystalline nickel was present in all traces of the reduced catalyst.

The intensity of this line is proportional to the weight fraction of diffracting nickel crystallites in the catalyst since if W_1 is small, the expression (*9*)

$$I_1 \propto \frac{W_1}{\rho_1[W_1(\mu_1 - \mu_2) + \mu_2]} \qquad (1)$$

reduces to

$$I_1 \propto \frac{W_1}{\rho_1 \mu_2} \qquad (2)$$

Here ρ_1 and W_1 are the density and weight fractions of diffracting nickel in the catalyst. The X-ray mass absorption coefficients for nickel (μ_1) and the zeolite (μ_2) were calculated as 48.3 and 33.1 cm^2 g^{-1}. The relative line intensity for a reduced catalyst with maximum nickel loading and a standard physical mixture comprising zeolite and pure crystalline nickel powder was measured. After correcting for sample weights the relative intensity was 1:4 in favor of the standard mixture. It was therefore concluded that 25% of the nickel in the catalyst was in the form of crystallites >50 Å diameter, which is the minimum size required before a crystal will contribute significantly to the intensity of an X-ray diffraction line (*10*).

Kinetic Analysis

There is evidence to suggest that reforming isomerizations over Pt/alumina bifunctional reforming catalysts proceed in three stages (*2–7*). Since the catalyst used in this work was found to be bifunctional, in that

isomerization activity over the unmodified zeolite and pure nickel was negligible in each case, a reaction sequence within the above framework was envisaged here, vis.

dehydrogenation $n\text{-pentane} \xrightarrow{Ni} n\text{-pentene} + H_2$

isomerization $n\text{-pentene} \xrightarrow{proton}$ i-pentene

hydrogenation $H_2 +$ i-pentene $\xrightarrow{Ni}$ i-pentane.

The equilibrium constants for these reactions are denoted by K_d, K_i, and K_h, respectively. Each step can be split up into a number of substeps to indicate the usual processes of adsorption, surface reaction, and desorption. Langmuir–Hinshelwood rate expressions were derived for each substep assuming it to be rate controlling. Rate expressions describing all the hydrogenation and dehydrogenation substeps indicate that the rate depends on the total pressure. This is so when single- and dual-site reaction sequences are considered, and also for hydrogen adsorption onto nickel with and without dissociation. It is likely that carboniogenic isomerization of the *n*-olefin proceeds using only one proton site, and rate expressions describing the three substeps of a single-site isomerization sequence of the pentene show that if any one of these is rate controlling then the rate will be independent of the total pressure. However, it is assumed that pentanes and hydrogen possess negligible affinity for the proton sites in comparison to the olefins.

An initial screening of substeps was possible by examining the effect of total pressure on conversion at 295 and 319°C at constant space velocity. A H_2/nC_5 inlet molar ratio of 13.7/1 was used for the lower temperature runs, while a molar ratio of 8.4/1 was used at the higher temperature. The results are illustrated in Figs. 4 and 5. Only ca. 10% of the converted *n*-pentane was cracked at 295°C compared to a maximum of 45% at 319°C. There was a decreasing tendency for cracking to occur with increasing total pressure whereas conversions to isomer remained constant at each temperature. The pressure independence of conversion to isomer suggested the rate-determining step to be contained within the isomerization sequence as appears to be the case with nonzeolitic reforming catalysts (*4*, *7*). In consequence it was necessary to discriminate between the three possible rate-controlling substeps constituting the isomerization sequence, as represented by the equations

n-Pentene adsorption

$$R = \frac{k_a K_d (P_1 - P_2/K)}{P_3 + (1/K_7K_h)(1/K_6 + 1)P_2}, \quad (3)$$

Surface isomerization

$$R = \frac{k_i K_5 K_d (P_1 - P_2/K)}{P_3 + K_5K_dP_1 + P_2/K_7K_h}, \quad (4)$$

i-Pentene desorption

$$R = \frac{k_d K_5 K_6 K_d (P_1 - P_2/K)}{P_3 + K_5K_d(1 + K_6)P_1}. \quad (5)$$

These equations were written in partial pressures of pentanes and hydrogen by making use of the equilibrium relations between pentanes, pentenes, and hydrogen. Here K_5, K_6, K_7, and k_a, k_i, k_d are the thermodynamic equilibrium constants and forward rate constants for the adsorption, surface isomerization, and desorption substeps respectively and K is the equilibrium constant for the overall isomerization of *n*-pentane.

Rate data were collected by varying the partial pressures of *n*-pentane P_1, i-pentane P_2, and hydrogen P_3, up to maximum partial pressures of 17.2×10^4, 6.1×10^4, and 180×10^4 N m^{-2} respectively. The data were collected according to an experimen-

tal design consisting of the coordinates of a cube superimposed on the vertices of an octahedron (*12*). The design was made rotatable by choosing the distance of the vertices of the octahedron from the design central point to equal 1.68. Replication at the central point in the design allowed an estimate of the pure error variance in the rate to be obtained. In order to reduce the effects of time trends on the error variance, the design matrix was divided into three blocks, with all experiments in one block being completed before starting another block. Such experimental designs offer several advantages which are well documented elsewhere (*12*).

Rate data were collected according to the design at 295, 301, and 319°C, using a catalyst containing maximum nickel loading. These combinations of low temperature and high hydrogen partial pressure gave rise to good isomerization activity and undetectable deactivation, thus indicating that carbonium ion cracking reactions which would deposit carbon are unimportant.

Both linear and nonlinear regression techniques were used for data fitting. For the linear analysis, the equations were transposed to the general form

$$\frac{P_1 - P_2/K}{R} = b_1P_1 + b_2P_2 + b_3P_3. \quad (6)$$

Reciprocal rate quantities were minimized and a degree of fit was obtained by computing the ratio of the lack of fit mean square to the pure error mean square and comparing with the tabulated F statistic. The lack of fit sum of squares was calculated as the difference between the residual and the pure error sums of squares. Data at each temperature were processed separately on an IBM 370 computer and the results are presented in Table 2. However, this analysis requires the reciprocal rate quantities to satisfy certain conditions (*13*). As a consequence of this and for completeness, the data were fitted to the untransformed rate equations using the Nelder and Mead Simplex procedure with quadratic acceleration (*14, 15*). The results of the nonlinear analysis are given in Table 3.

DISCUSSION

Nickel Dispersion

Figure 1 indicates that the amount of CO retained at 100 Torr is directly proportional to the catalyst nickel loading. This is an indication that the degree of dispersion of the nickel in the catalyst remains virtually the same regardless of metal loading. It is also evident from the figure that each nickel atom retains an average of 1.9 molecules of CO. Since it has been shown that 25% of the nickel is in the form of diffracting crystallites, such a high adsorbed CO ratio suggests that most of the remaining nickel atoms take part in CO adsorption. If it is assumed that an average diffracting crystallite is a cube with a 300-Å edge (typical value taken from electron micrographs), a simple calculation reveals that each exposed nickel atom retains an average of

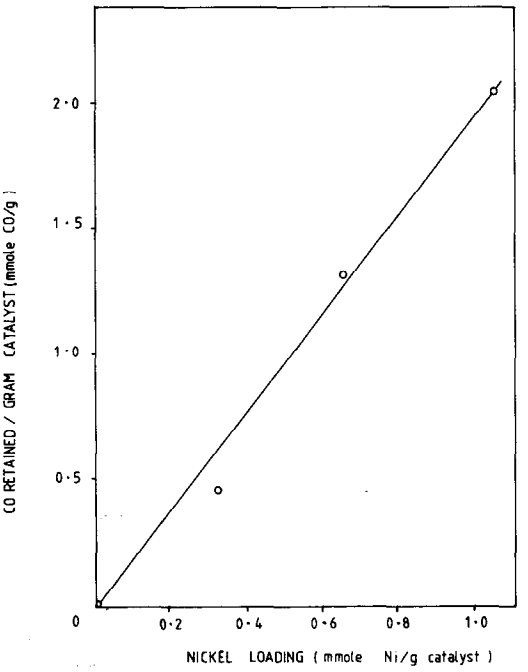

FIG. 1. Carbon monoxide retained at 100 Torr vs catalyst nickel loading.

about 2.5 molecules of CO. This takes into account both the surface atoms of the crystallites and the nondiffracting nickel. A bonding mode in which CO-bridged species are adsorbed between adjacent nickel atoms, already carrying linearly adsorbed CO molecules, would be expected to predominate at 100 Torr (*16*). This would give rise to a CO/Ni ratio of 2/1. It is also postulated that some carbon monoxide is bridge-bonded between "rows" of Ni atoms:

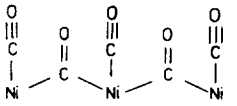

This arrangement results in between two and three CO molecules being adsorbed by each Ni atom. Such a mode of bridge-bonding requires there to be adjacent nickel atoms, and thus the nondiffracting nickel is envisaged as having monolayer character. Numerous electron micrographs revealed that the nickel crystallites formed predominantly at the surface of the host zeolite crystals. Since the remaining nickel appears to be of monolayer character, it would seem that all of the reduced nickel lies at the zeolite surface.

A tentative description of the reduction process is that the nickel ions are first reduced in the surface region on the zeolite crystal, leaving a high concentration of protons in the surface region. Counterdiffusion of nickel ions and protons then takes place, supplying more nickel ions to the surface region of the zeolite crystal which are subsequently reduced to zero-valent nickel at the surface. The intracrystalline regions of the zeolite thus become richer in protons at the expense of the nickel ions, and the surface of the zeolite crystals is able to accumulate zero-valent nickel.

As a cautionary note it should be realized that the CO adsorption method for the determination of nickel surface area could lead to misleading results if not approached with great care. The thermodynamic conversion to nickel carbonyl is very heavily favored by high pressure and low temperatures (*17*), the rate of formation reaching a maximum at 75°C (*18*). The presence of a high concentration of nickel carbonyl could provide a mechanism for redistribution of nickel on the catalyst, and conditions should be chosen so as to preclude this possibility.

Catalytic Activity

Figure 2 shows that conversion to isomer increases up to about 320°C, after which it decreases. This effect is most noticeable with the most highly loaded catalyst and the cracking pattern obtained with this catalyst (Table 1A) shows the high methane levels which are characteristic of hydrogenolysis over nickel (*19*). The typical patterns shown in Table 1B were all obtained at conversions to light hydrocarbons of <2% and therefore represent initial rates. Again the figures show the high methane levels caused by hydrogenolysis at the terminal methyl group, but with less degradation to methane than the higher temperature conversion levels of Table 1A. However, successive demethylation would require at

TABLE 1

A. Distribution of light hydrocarbons with temperature

P_{nC_5} (atm)	P_{H_2} (atm)	Temp. (°C)	Distribution (mole%)			
			C_1	C_2	C_3	C_4
1.5	6.3	316	60.0	4.0	10.7	25.3
		333	68.9	6.3	10.7	14.1
		364	88.1	7.1	3.2	1.6

B. Distribution of Light Hydrocarbons with Hydrogen Pressure

P_{nC_5} (atm)	P_{iC_5} (atm)	P_{H_2} (atm)	Temp. (°C)	Rate of C_5 conversion to light hydrocarbons[a] (mole hr^{-1} g^{-1})	Distribution (mole%)			
					C_1	C_2	C_3	C_4
1.2	0.4	10.9	319	92.4×10^{-5}	51.3	3.3	8.7	36.7
1.2	0.4	13.4		51.8×10^{-5}	47.8	3.7	8.4	40.1
1.3	0.4	17.7		24.5×10^{-5}	44.1	4.3	8.8	42.8

[a] Rates obtained at conversion to light hydrocarbons of <2%.

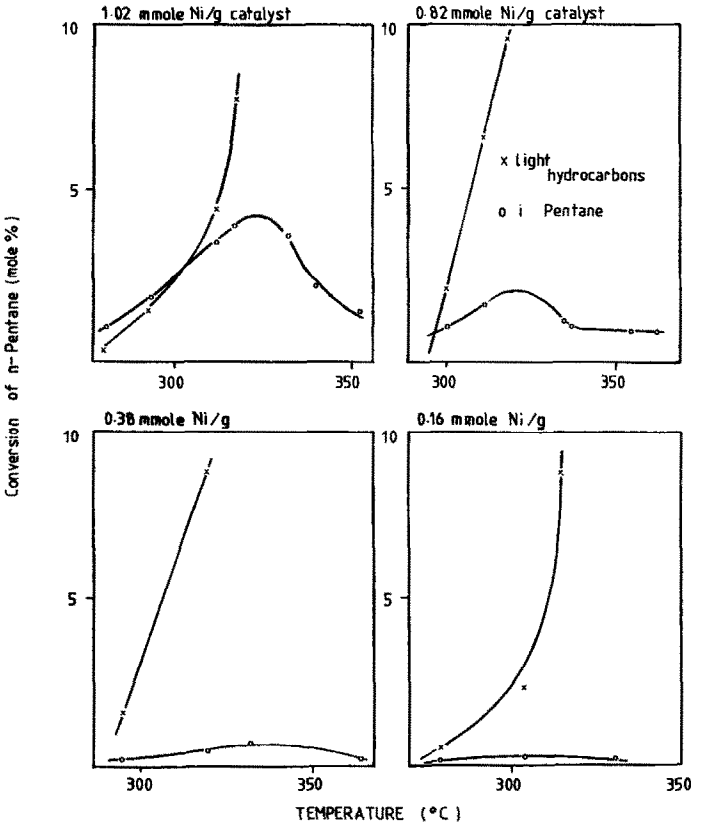

FIG. 2. Percentage conversion on nC_5 to iC_5 and light hydrocarbons vs temperature for catalysts with various nickel loadings.

least 50 mole% methane in the product stream. Therefore there is a small contribution through splitting of nonterminal carbon–carbon bonds at the higher hydrogen pressures. The rates of light hydrocarbon formation were always strongly inhibited by increasing hydrogen partial pressure. Examination over the whole range of rate data indicated that the rate of pentane conversion to light hydrocarbons was an inverse function of P_{H_2}, which is another characteristic of hydrogenolysis (*20*).

Catalysts were reduced at 480–500°C which produces a predominantly Brønsted acid form of the zeolite (*21*).

It can be seen from Fig. 3 that the introduction of the nickel proton couple produces a more than linear increase in activity for isomerization. Similar increases in activity have been observed for reactions catalyzed by the Brønsted acid sites of Y-type zeolites containing no nickel. For example, replacement of sodium ions with ammonium ions followed by deamination led to a dramatic increase in cumene cracking activity between exchange levels of 25–70% (*22*). In another study (*23*) catalyst activity for *p*-xylene isomerization was found to increase with proton concentration, the greatest increase being between 60 and 100% sodium exchange. The increase in isomerization activity was ascribed to the intrazeolite protons and their occupancy of different exchange sites within the zeolite.

The catalyst used in this work was essentially a Na^+H^+Y catalyst containing nickel with the nickel dispersion being independent of nickel loading. Therefore the evidence points to the increase in isomeriza-

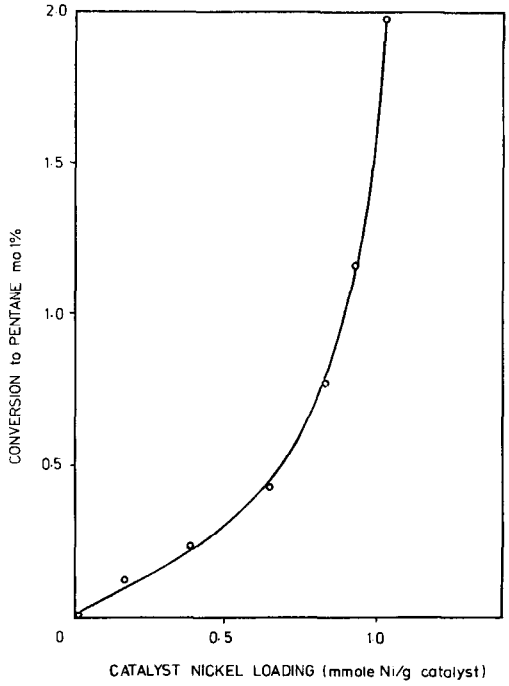

FIG. 3. Conversion to i-pentane vs catalyst nickel loading at 295°C.

tion activity with nickel loading as being due to the accompanying protons.

If the specific activity per unit volume of zeolite crystallite is linearly related to the proton concentration X, and if the protons are uniformly distributed through the zeolite and there is no diffusional limitation on the accessibility of olefin to protons, then the reaction rate should increase linearly with X. However, if there is a strong diffusional limitation the rate will vary as $X^{1/2}$, since increasing X increases the Thiele modulus without changing the particle size. In fact, the isomerization rate (Fig. 3) varies approximately as X^2 which, although reflecting the increasing activity of the active sites, is also taken to indicate that there is no internal diffusional limitation.

Kinetics

The independence of conversion to isomer with total pressure is not a conclusive test that an isomerization substep is rate controlling. This is because the apparent degree of dependence of the reaction rate on total pressure for each hydrogenation–dehydrogenation substep is governed by the relative magnitude of the groups of constants in the relevant equations. Nevertheless, the pressure independence of conversion is apparent over a substantial pressure range at both temperatures.

Taken together with the indications that conversion is dependent upon the loading of the intrazeolite protons, it is concluded that the rate-determining step is contained within the n-pentane isomerization sequence.

The linear regression analysis (Table 2) shows b_1 to be highly insignificant for the three models at each temperature, and therefore it contributes nothing to the fit. At 295°C b_2 is just insignificant for both models whereas at 308°C it is significant for the model which assumes adsorption of pentene on proton sites is rate controlling but just insignificant for the model in which the surface reaction is rate controlling. High significance for b_2 is observed at 319°C; b_3 is highly significant wherever it appears and

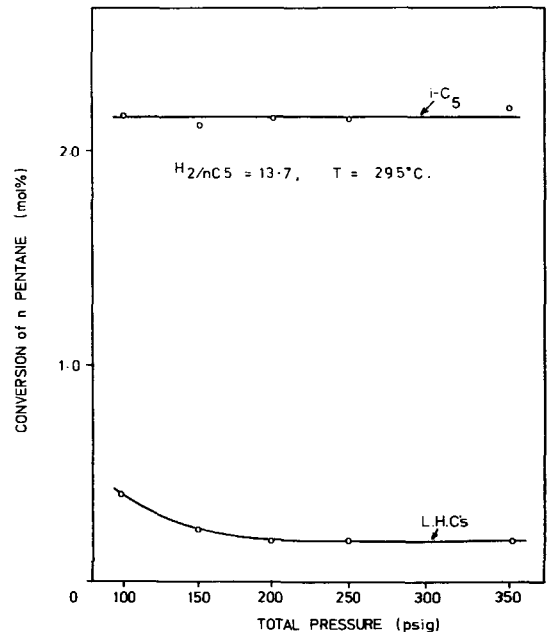

FIG. 4. Conversion of n-pentane to i-pentane and light hydrocarbons vs total pressure at 295°C.

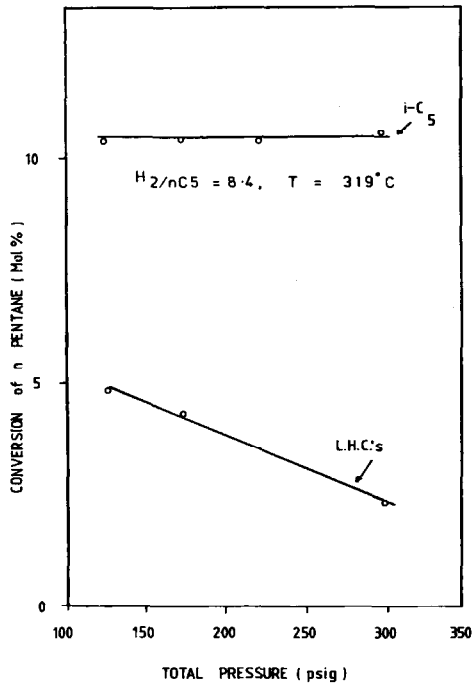

FIG. 5. Conversion of *n*-pentane to i-pentane and light hydrocarbons vs total pressure at 319°C.

must be included. Comparison of the F ratio for an assumed slow desorption step with the ratios for the other two models shows that, in general, b_2 should be included. The effect of leaving b_2 out is most marked at the highest temperature where the F ratio increases from 1.58 to 2.37. The tabulated F statistic is 3.7 at the 10% level of significance, and therefore there is no evidence of lack of fit at any temperature.

Response variable transformation is a common tool used in reaction kinetics to simplify the processing of rate data (e.g., (*13*)). The validity of the results, however, depends upon the error variance of the transformed group being constant and normally distributed with zero mean. The experimental design used here requires that the pure error variance obtained at the 000 coordinate is representative of the error variance at the remaining coordinates. These assumptions were probably not too far from the truth since errors in rate measurements were comparable irrespective of the absolute magnitude of the rate. Also, the measured rates did not differ over an excessively wide range. This would be expected to lead to a reciprocal rate response group with a reasonably normally distributed and constant error variance provided the absolute rate data satisfied these conditions. For completeness though, the regression coefficients were also obtained by nonlinear regression, the reaction rate terms, R and $\hat{R}$, being minimized. Here, R and $\hat{R}$ are the observed and predicted reaction rates,

TABLE 2

Linear Regression Analysis of Experimental Data from Equation (6)[a]

Model	T (°C)	b_1	b_2	b_3	F ratio
Adsorption			1532*	149(±49)	1.43 Accept?
Surface isom.	295	−582**	1921*	192(±92)	1.44 Reject
Desorption		−200.9**		205(±94)	1.58 Reject
Adsorption			295(±289)	77(±7)	2.34 Accept
Surface isom.	308	42**	267*	73(±15)	2.48 Reject
Desorption		95**		76(±12)	2.62 Reject
Adsorption			449(±224)	46(±6)	1.58 Accept
Surface isom.	319	16**	434(±282)	45(±12)	1.70 Reject
Desorption		146.3*		45(±13)	2.37 Reject

[a] Significance and confidence intervals Based on $t_{0.95}$.

* Insignificant.

** Highly insignificant.

TABLE 3

Nonlinear Regression Analysis of Experimental Data

Model	T (°C)	b_1	b_2	b_3	
Adsorption			1266(±1063)	138(±26)	Accept
Surface isom.	295	−297**	1331(±1091)	166(±61)	Reject
Desorption		−276**		199(±85)	Reject
Adsorption			386(±239)	74(±6)	Accept
Surface isom.	308	51**	365(±241)	69(±13)	Reject
Desorption		96**		76(±17)	Reject
Adsorption			486(±209)	45(±5)	Accept
Surface isom.	319	1**	489(±196)	45(±9)	Reject
Desorption		71**		51(±14)	Reject

* Insignificant.
** Highly insignificant.

and the resulting coefficients are given in Table 3.

b_1 is insignificant wherever it appears. b_2 is always significant, and b_3 is always highly significant. These results support the conclusion that only a two-parameter model is necessary. The estimates of b_3 are the same as those obtained from the linear analysis to within a few percent. However estimates of b_2, where significant, differ by up to 30% depending upon the method of analysis used. Nevertheless, values of b_2 always lie within the confidence bands of corresponding estimates from the linear analysis.

In the two-parameter equation describing the adsorption step as rate controlling, the constant $k_a(=kX)$ is the product of the forward adsorption rate constant and the concentration of active sites in the zeolite. The partial regression coefficient, b_3, is then equal to $1/kK_dX$ and thus a value of kX can be calculated at all three temperatures providing values of K_d at these temperatures are available. This allows an Arrhenius plot to be constructed from which an explicit activation energy can be extracted. It must be assumed, though, that the concentration of active sites remains constant over the whole temperature range. Values of K_d, the equilibrium constant for the dehydrogenation of *n*-pentane to pent-2-ene, were calculated from thermodynamic data (*24*). An Arrhenius plot of log (kX) vs $1/T$ was plotted from which an estimated activation energy of 3 kcal/mole was extracted. An apparent activation energy was also obtained by assuming Rate = k ($C_{\text{reactants}}$, C_{products}). Reaction rates were measured at each temperature under the same concentrations of reactants and products and plotted in Arrhenius fashion (Fig. 6). The apparent activation energy extracted from the plot was 28 ± 4 kcal/mole, a similar value to that reported for activation energies over nonzeolitic reforming catlaysts.

The activity for isomerization of the catalyst used in this work was found to be comparable to the activity of Pt/alumina catalysts (*4*, *7*) when brought to the same temperature basis of around 320°C. However, the latter tend to retain higher selectivity for isomerization at the higher temperatures.

CONCLUSIONS

The results reported here are consistent with the isomerization mechanism proposed for other dual-function catalysts, no-

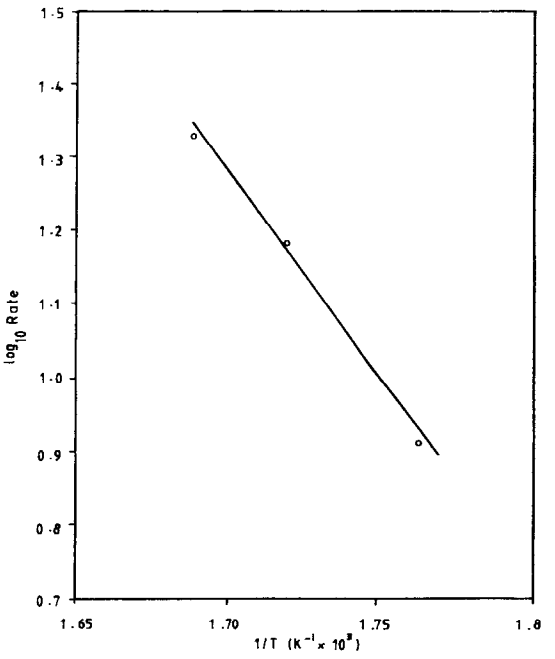

FIG. 6. Arrhenius plot.

tably platinum on alumina. The olefin formed by dehydrogenation on the dispersed nickel is assumed to migrate rapidly to zeolite acid sites where it is adsorbed and undergoes an ionic rearrangement.

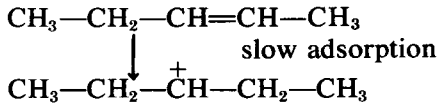

Other steps in the isomerization sequence—hydride shift, double-bond formation, and desorption of i-pentane—are assumed fast. The increase in isomerization activity with nickel loading is noteworthy and light hydrocarbons are principally formed by hydrogenolysis over nickel. An unanswered question remains as to how the activity of the catalyst depends on the particular metal introduced into the zeolite and its mode of reduction.

REFERENCES

1. Kouwenhoven, H. W., and Van Zijll Langhout, W. C., *Chem. Eng. Progr.* **67(4)**, 65 (1971).
2. Mills, G. A., Hienemann, H., Milliken, T. H., and Oblad, A. G., *Ind. Eng. Chem.* **45**, 134 (1953).
3. Weisz, P. B., and Swegler, E. W., *Science* **126**, 31 (1957).
4. Sinfelt, J. H., Hurwitz, H., and Rohrer, J. C., *J. Phys. Chem.* **64**, 892 (1960).
5. Sinfelt, J. H. Hurwitz, H., and Rohrer, J. C., *J. Catal.* **1**, 481 (1962).
6. Schmerling, L., *Ind. Eng. Chem.* **45**(1), 447 (1953).
7. Hosten, L. H., and Froment, G. F., *Ind. Eng. Chem. Process Des. Develop.* **10**(2), 280 (1971).
8. Brooks, C. S., and Christopher, G. I. M., *J. Catal.* **10**, 211 (1968).
9. B. D. Cullity, "Elements of X-Ray Diffraction," p. 390. Addison–Wesley, Reading, 1959.
10. Spenadel, L., and Boudart, M., *J. Phys. Chem.* **64**, 204 (1960).
11. Eggertsen, F. T., and Roberts, R. M., *Anal. Chem.* **22**, 924 (1950).
12. Hunter, J. S., *Chem. Eng. Progr. Symp. Ser.* **56**(31), 10 (1960).
13. Hougen, O. A., and Watson, K. M., "Chemical Process Principles, Part 3," p. 941. Wiley, New York, 1964.
14. Nelder, J. A., and Mead, R., *Comput. J.* **7**, 308 (1965).
15. Keele, *in* "Optimaztion" (R. Fletcher, Ed.), p. 259, Academic Press, New York, 1969.
16. Yates, J. T., and Garland, C. W., *J. Phys. Chem.* **64**, 617 (1961).
17. Densham, A. B., Cooper, L. S., and Tanner, M. W., *in* "Materials Technology in Steam Reforming Process" (C. Edeleanu, Ed.), p. 343. Pergamon, Oxford, 1966.
18. Goldberger, W. M., and Othmer, D. F., *Ind. Eng. Chem. Process Des. Develop.* **2**(3), 203 (1963).
19. Kikuchi, E., and Yoshiro, M., *J. Catal.* **15**, 217 (1969).
20. Kikuchi, E., Tsurumi, M., and Morita, Y., *J. Catal.* **22**, 226 (1971).
21. Turkevich, J., and Ono, Y., *in* "Molecular Sieve Zeolites II" (E. M. Flanigen and L. B. Sand, Eds.), Advances in Chemistry Series 102, p. 315. Amer. Chem. Soc., Washington, D.C., 1971.
22. Tsutsumi, K., and Takahashi, H., *J. Catal.* **24**, 1 (1972).
23. Ward, J. W., and Hansford, R. C., *J. Catal.* **13**, 364 (1969).
24. Rossini, F. D., "Selected Values of Physical Properties of Hydrocarbons and Related Compounds." Carnegie Press, Pittsburgh, 1953.